Solvent-Mediated Enhancement of Additive-Controlled Crystallization

Ouassef Nahi,[*a] *Alexander N. Kulak,*[a] *Alexander Broad,*[b] *Yifei Xu,*[a] *Cedrick O'Shaughnessy,*[a] *Olivier J. Cayre,*[c] *Sarah J. Day,*[d] *Robert Darkins,*[b] *and Fiona C. Meldrum*[*a]

[a] School of Chemistry, University of Leeds, Woodhouse Lane, Leeds, LS2 9JT, UK

[b] London Centre for Nanotechnology, Department of Physics and Astronomy, University College London, Gower Street, London WC1E 6BT, UK

[c] School of Chemical and Process Engineering, University of Leeds, Woodhouse Lane, Leeds, LS2 9JT, UK

[d] Diamond Light Source, Harwell Science and Innovation Campus, Harwell, Didcot, Oxfordshire, OX11 0DE, UK

EMAIL ADRESSES

Ouassef Nahi: pmona@leeds.ac.uk

Alexander N. Kulak: a.kulak@leeds.ac.uk

Alexander Broad: a.broad.17@ucl.ac.uk

Yifei Xu: y.xu4@leeds.ac.uk

Cedrick O'Shaughnessy: c.oshaughnessy@leeds.ac.uk

Olivier J. Cayre: o.j.cayre@leeds.ac.uk

Sarah J. Day: sarah.day@diamond.ac.uk

Robert Darkins: r.darkins@ucl.ac.uk

Fiona Meldrum: f.meldrum@leeds.ac.uk

KEYWORDS

Calcium carbonate, magnesium, composite, amino acid, biomineral, calcite.

ABSTRACT

Soluble additives are widely used to control crystallization processes, modifying the morphologies, sizes, polymorphs, and physical properties of the product crystals. Here, a simple and versatile strategy is shown to significantly enhance the potency of soluble additives, ranging from ions and amino acids to large dye molecules, enabling them to be effective even at low concentrations. Addition of small amounts of miscible organic co-solvent to an aqueous crystallization solution can yield enhanced morphological changes and an order of magnitude increase of additive incorporation within single crystals — a level that cannot be achieved in pure aqueous solution at any additive concentration. The generality of this strategy is demonstrated by application to crystals of calcium carbonate, manganese carbonate and strontium sulfate, with a more pronounced effect observed for co-solvents with lower dielectric constants and polarities, indicating a general underlying mechanism that alters water activity. This work increases the understanding of additive/crystal interactions and may see great application in industrial-scale crystal synthesis.

INTRODUCTION

From biomineralization to synthetic systems, soluble additives offer a powerful means of controlling crystallization processes. In this way, it is possible to control polymorph, size and shape of a crystal. In addition, occlusion of guest additives within crystal hosts can create composite materials with new physical and chemical properties.[1-3] Given the importance of calcium carbonate to the environment, biology and industry, a large body of work has focused on the effects of soluble additives on its crystallization ranging from elemental ions (Mg^{2+}, Sr^{2+}

and Li^+),[4-8] to small molecules such as amino acids, to macromolecules including proteins, polysaccharides and block copolymers[9-14] and even particulate additives.[14-16] These studies have provided information about the mechanisms underlying the interactions between additives and calcium carbonate crystals, where morphology changes can be rationalized in terms of preferential binding of the additives to the acute or obtuse steps on the crystal surface. Incorporation of additives within host crystals generates hybrid materials with enhanced hardness,[17] magnetism,[18] and optical properties.[19, 20]

Crystallization is also necessarily affected by the nature and composition of the solvent. In aqueous solution, incorporation of calcium and carbonate ions into the crystal lattice requires the displacement of water molecules adsorbed at the crystal surface and dehydration of the ions themselves.[21-23] The binding of additives is subject to similar constraints. Changing the solvent composition therefore promises the ability to easily tune crystallization processes by modulating the interactions of the additive with the crystal surface, as well as regulating precipitation kinetics and mineral and additive solubility.[24, 25] Indeed, addition of organic solvents to an aqueous crystallization solution can shift the polymorph from the thermodynamically stable calcite polymorph toward the metastable vaterite and aragonite phases,[26-28] although changes in the $CaCO_3$ crystallization pathways is only achieved at relatively high co-solvent/water ratios (typically over 50 vol%).

Here, we explore the effects of organic co-solvents on calcium carbonate precipitation in aqueous solutions and show that just small amounts (less than 15 vol%) vastly increase the capacity of additives to tune crystal morphologies and create single crystal nanocomposites through their incorporation within calcite single crystals. Using model additives ranging from magnesium ions, to amino acids and ultimately large dye molecules, we also demonstrate that

the co-solvent addition to the crystallization solution can also promote additive incorporation within calcite single crystals. The greatest enhancement is observed for the co-solvents with the lowest dielectric constants and polarities, and we demonstrate identical behavior for a range of inorganic crystals, indicating a general underlying mechanism. This straightforward methodology provides an alternative to current methods that achieve habit changes and occlusion by controlling the chemical structure of additives,[14, 29, 30] where alteration of the physico-chemical properties of the solvent offers a simpler, more versatile, and scalable means of controlling crystallization processes at low additive concentrations, and achieving incorporation levels way beyond those possible in aqueous solutions.

RESULTS

Effects of water/ethanol mixtures on calcium carbonate precipitation

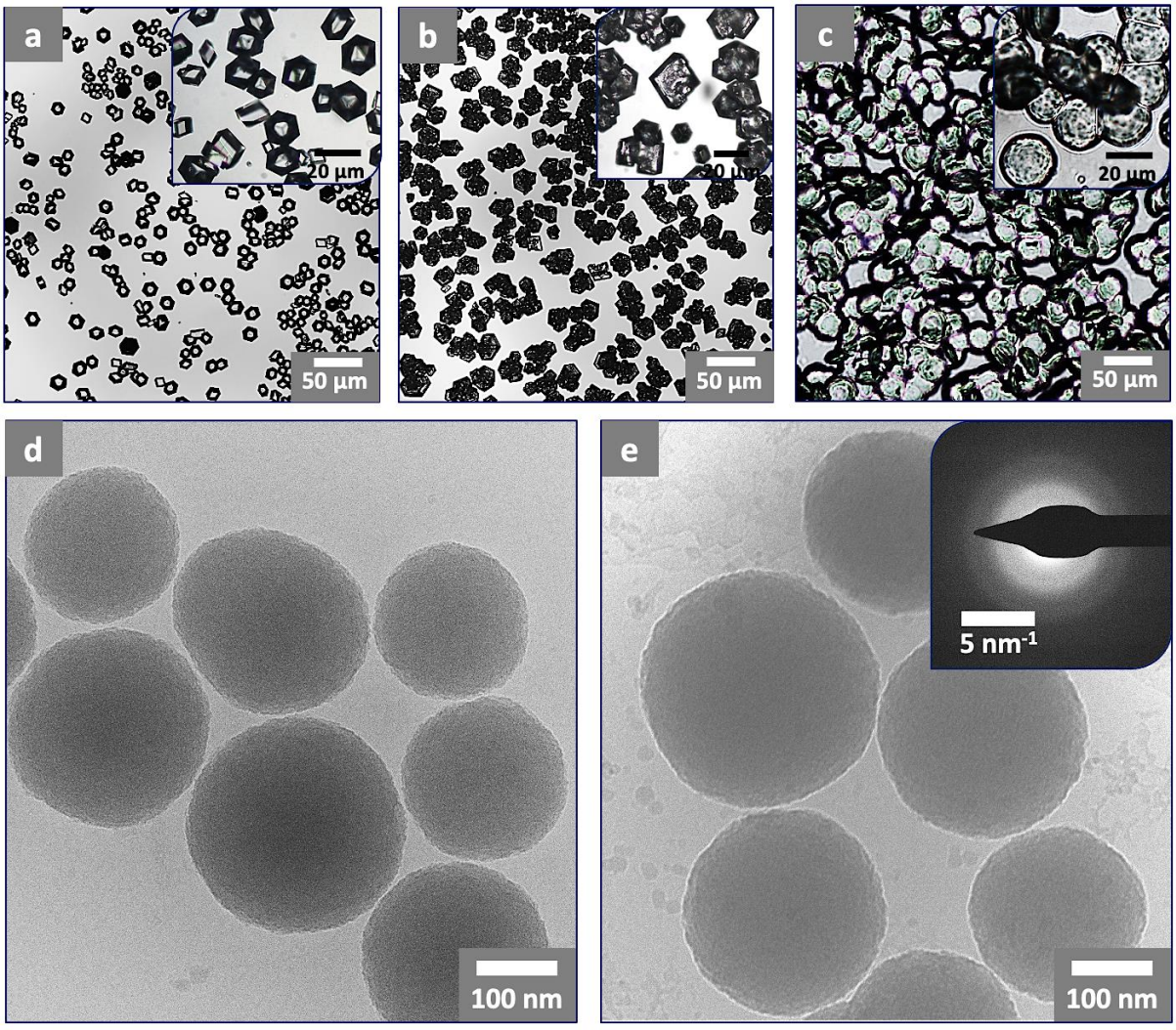

Figure 1. Calcium carbonate precipitated in water/ethanol solution containing [Ca^{2+}] = 10 mM. (a) Calcite formed at ≤ 25 vol% ethanol, (b) calcite formed at 30-50 vol% ethanol, and (c) vaterite formed at > 50 vol% ethanol. Inset in (a) is a micrograph of calcite crystals precipitated in pure aqueous system and insets in (b) and (c) are higher magnification images of the precipitated crystals in the presence of ethanol in solution. Cryo-TEM micrographs of amorphous calcium carbonate (ACC) particles precipitated in (d) a pure aqueous system, and (e) in 20 vol% ethanol. The inset is a SAED pattern showing diffuse rings indicative of amorphous material.

The effects of binary solvent mixtures on calcium carbonate precipitation were investigated. In the first instance, using the ammonium diffusion method,[31] phase pure rhombohedral calcite

crystals precipitated in pure aqueous solution at [Ca^{2+}] = 10 mM (Figure 1a and Figure S1). Introduction of ethanol changed the habit of the calcite crystals from rhombohedra with smooth {104} faces (≤ 25 vol% ethanol) to hopper crystals with pits in the centers of their faces (30 – 50 vol% ethanol) (Figure 1b and Figure S1) and vaterite formed at over 50 vol% ethanol (Figure 1c). Hopper morphologies are characteristic of diffusion-limited growth, where the vertices of a crystal are exposed to higher concentrations of solutes than the center of the faces, giving rise to faster growth.[27] Investigation of the early stages of mineralization using Consistent with previous work,[32, 33] cryogenic Transmission Electron Microscopy (cryo-TEM) revealed that amorphous calcium carbonate (ACC) was the first structure formed in all cases (Figure 1d-e), and that stability of this precursor phase was enhanced for ethanol contents above 50 vol% (Figures S1 and S2).[34, 35]

Incorporation of Brilliant Blue R dye within calcite in water/ethanol mixtures

Precipitation of calcium carbonate in the presence of BBR (Brilliant Blue R, a blue dye) from aqueous solution yielded pale blue rhombohedral calcite crystals, indicating limited interaction with the calcite surface and low levels of occlusion (Figure 2a). The amount of BBR occluded was determined by dissolving the crystals in buffered solution,[36] and quantifying the released dye using UV-Visible spectrophotometry (UV-Vis) (Figure 2l). The amount of $CaCO_3$ present in the samples was measured using Atomic Absorption Spectroscopy (AAS), thereby giving the ratio of [BBR] to $CaCO_3$. Solutions containing [Ca^{2+}] = 10 mM and [BBR] = 0.5 mM contained 0.75 wt% BBR, and higher [Ca^{2+}] = 20 mM increased occlusions levels to 1.2 wt%. This increase in occlusion with supersaturation can be attributed to a faster growth rate, which ensures that the steps propagate around the adsorbed dye molecules before they can desorb.[37]

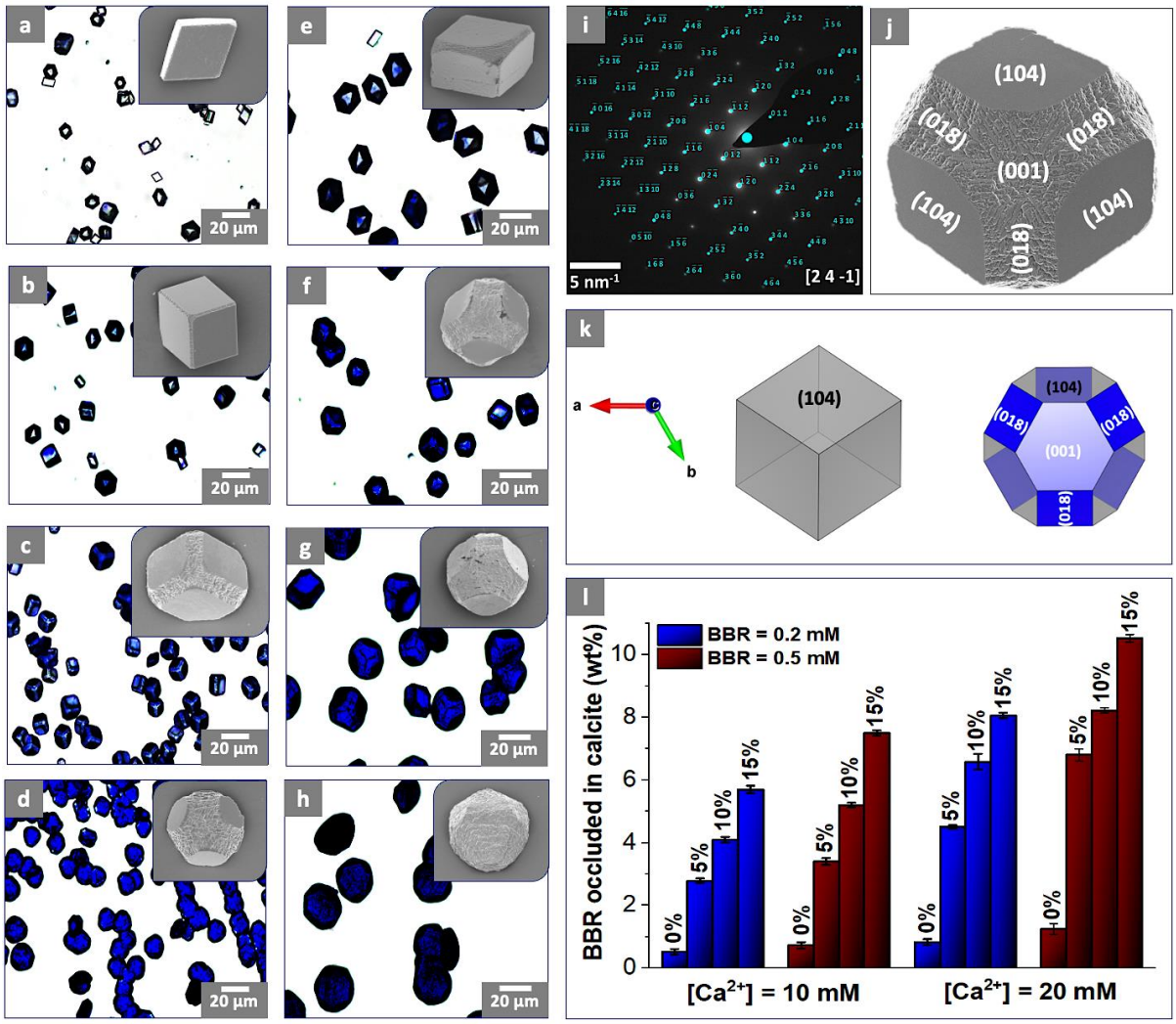

Figure 2. Optical images of calcite crystals precipitated at [BBR] = 0.2 mM and (a-d) [Ca^{2+}] = 10 mM, and (e-h) [Ca^{2+}] = 20 mM. These samples contain (a and e) 0 vol%, (b and f) 5 vol%, (c and g) 10 vol% and (d and h) 15 vol% ethanol. Insets are SEM micrographs of the product crystals. (i) Selected area electron diffraction (SAED) pattern of a thin section prepared using Focused Ion Beam (FIB) milling of a calcite crystal incorporating 10 wt% BBR, showing that it is a single crystal and (j) SEM micrograph showing the faces and pseudo-faces expressed by the binding of BBR to calcite. (k) Schematic representation of the morphological change of calcite from rhombohedra to platonic crystals. (l) Levels of incorporation of BBR in calcite precipitated at different dye, calcium and solvent concentrations.

Addition of small amounts of ethanol (5 – 15 vol%) significantly enhanced the incorporation of BBR and yielded uniformly-colored, dark blue calcite crystals, whose morphologies evolved from truncated rhombohedra to platonic forms as the ethanol concentration increased to 15

vol% (Figures 2b-d and Figure 2i). These shapes are indicative of preferential interaction of BBR molecules to the obtuse step edges of calcite (Table S1 and Figure 2j-k).[38] Notably, the composites are oriented with their [001] axis normal to the substrate. This is most likely induced by the adsorption the dye molecules on the substrate that direct the nucleation and orientation of crystals.[38, 39] Composite crystals precipitated in solutions comprising [Ca^{2+}] = 10 mM, [BBR] = 0.5 mM and 5 vol% ethanol contained ≈ 3.4 wt% of dye, which is ≈ 5 times higher than in pure water (Figure 2l). This increased further as the ethanol content increased, reaching 7.5 wt% BBR for [Ca^{2+}] = 10 mM, [BBR] = 0.5 mM and 15 vol% ethanol, corresponding to a 10-fold increase in occlusion as compared to pure water. Similar to the results obtained in aqueous solution, an increase in supersaturation in water/ethanol solutions enhanced the amount of BBR occluded (Figure 2f-h). Indeed, occlusion almost doubled from 3.5 wt% to 6.8 wt%, when [Ca^{2+}] was raised from 10 to 20 mM at [BBR] = 0.5 mM and 5 vol% ethanol.

Extension to alternative organic co-solvents

The study was then extended to methanol, propanol, iso-propanol (IPA) and dioxane, where these have distinct dielectric constants and polarities (Figure S3).[40, 41] As exemplified at reaction conditions [Ca^{2+}] = 20 mM, [BBR] = 0.2 mM and 10 vol% co-solvent, a small increase in dye occlusion from 0.83 wt% in pure water to 2.5 wt% was observed in solutions containing methanol. A significant enhancement occurred with propanol and IPA to 7 wt%, and dioxane supported the highest levels of BBR occlusion at 10 wt% under these conditions (Figure 3a-g). Greater BBR occlusion is also accompanied by more pronounced morphology changes in the crystals from calcite rhombs in the presence of methanol to platonic crystals for propanol, IPA and dioxane.

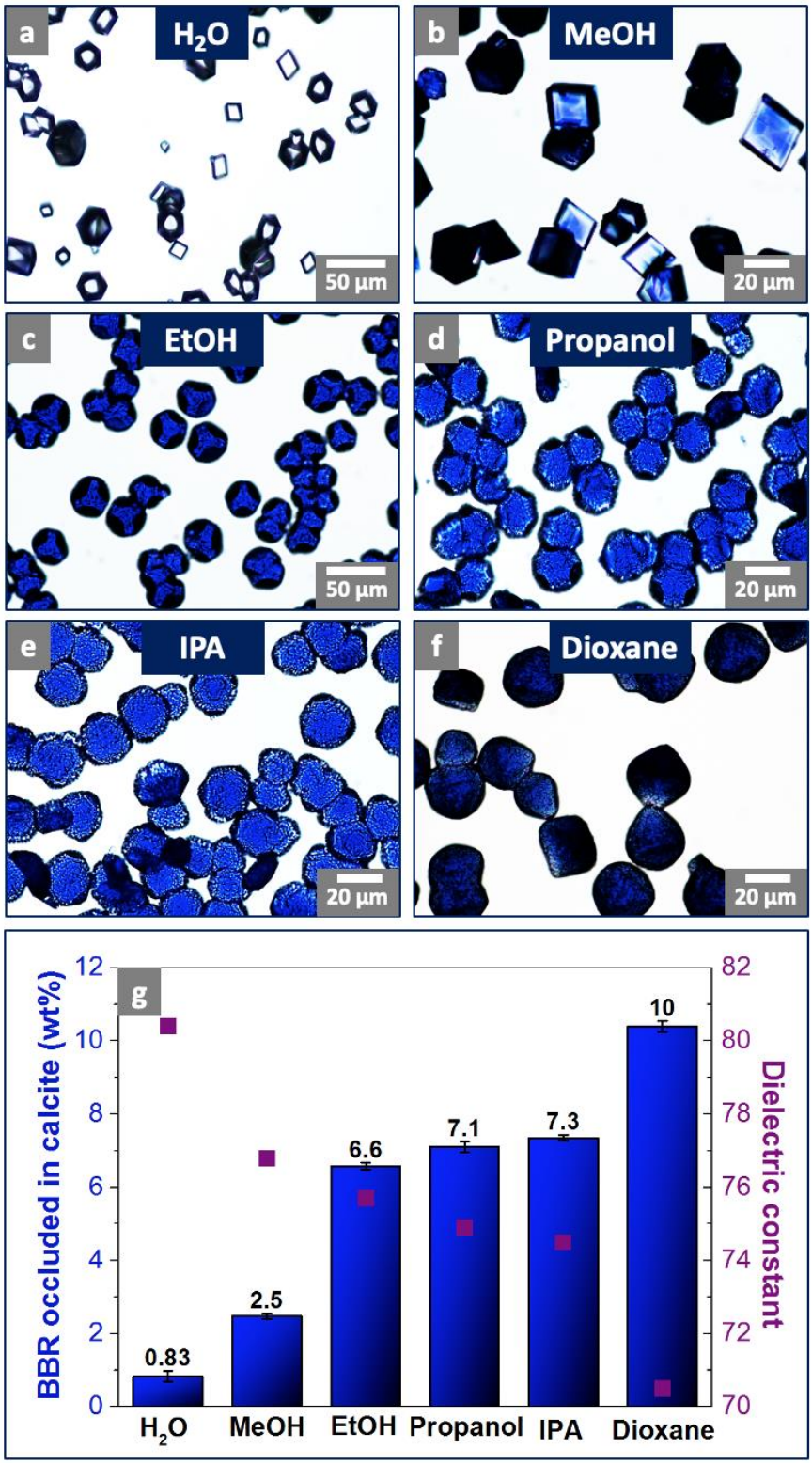

Figure 3. Calcite crystals precipitated in the presence of [Ca^{2+}] = 20 mM, [BBR] = 0.2 mM in (a) pure water and (b-f) 10 vol% of various organic co-solvents. (g) BBR occluded in calcite in pure water and in the presence of 10 vol% of various co-solvents in solution, and corresponding dielectric constants of the respective solution mixtures.

Importantly, the degree of dye incorporation and habit change correlate with the co-solvent properties, where methanol has the highest polarity and dielectric constant (*i.e.,* closest to that of pure water), while dioxane has the lowest (Figure 3g and Figure S3).[40, 41] Furthermore, since the co-solvents have different densities, they are present in solution at different molar concentrations: 10 vol% corresponds to 2.5 M for methanol, 1.3 M for IPA and propanol and 1.2 M for dioxane. At over double the concentration in the medium, methanol still has the least effect on dye occlusion, highlighting the pivotal role played by the physico-chemical properties of the solution.

Role of supramolecular assembly in BBR incorporation in calcite

It is well-established that the structural and chemical properties of organic molecules such as dyes can be affected by the pH, ionic strength, dielectric constant and polarity of the solution.[42-44] We therefore investigated the impact of ethanol on the structure of BBR. UV-Vis showed no significant changes in the characteristic absorbance peak of BBR (λ = 550 nm) in pure water or in solutions containing 20 vol% ethanol (Figure 4a-b and Figure S4a), while TEM revealed comparable BBR fibers with sizes ranging from 20 nm up to a micron in pure water and solutions containing ethanol (Figure 4c-d). These structures are expected due to the relatively low solubility of the dye in solution (1 mg mL^{-1}). Further, the UV-Vis-IR spectra of the dye solutions prepared in the presence of Ca^{2+} ions show only a slight decrease in the peak at 550 nm, which most likely arises from the complexation of the Ca^{2+} ions with the dye molecules (Figure S4b). This may contribute to the formation of dye aggregates in the mineralization solution (Figure 4e). Centrifuged dye solutions prepared in both water and ethanol/water mixtures also yielded only a slight decrease in absorbance intensity due to removal of the dye aggregates in solutions (Figure S4c-d).

The role of the BBR fibers on incorporation of the dye was further investigated by incubating a stock solution of 2 mM BBR and 10 vol% ethanol for 24 hours to allow for dye self-assembly. This solution was then introduced at a concentration of 0.2 mM of BBR and a corresponding 1 vol% of ethanol into the crystallization medium. Although many fibers of BBR were present in the mineralization solution (Figure 4e), limited incorporation of the dye into the crystals was achieved in solutions containing 1 vol% ethanol (Figure 4f). In contrast, when the same BBR solution was added to the crystallization solution ant the ethanol content adjusted to 10 vol%, calcite crystals of a dark blue color were formed (Figure 4g), which clearly indicate a significant level of occlusion of BBR in the crystals. These results demonstrate that the presence of self-assembled BBR molecules has little effect on incorporation.

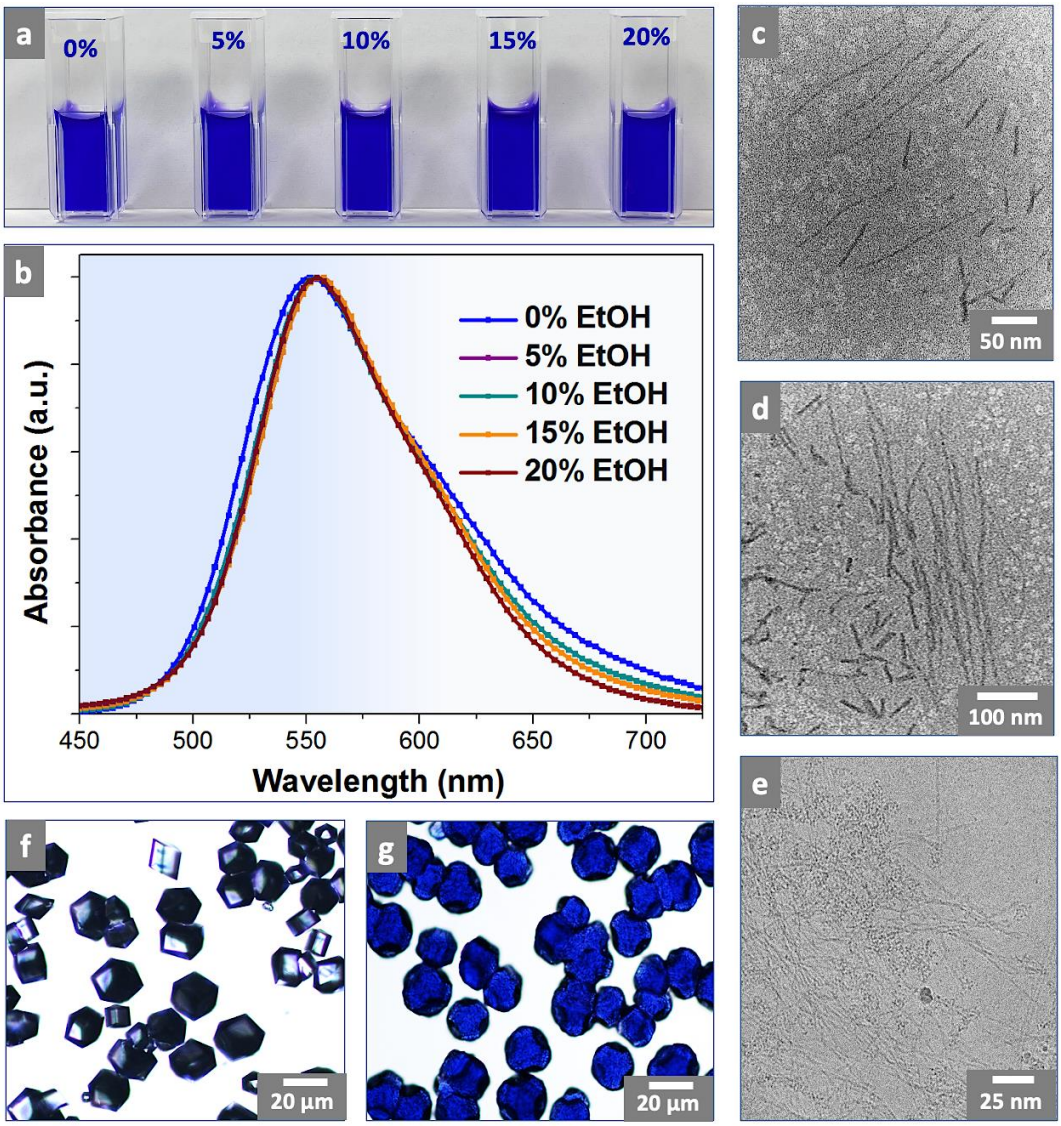

Figure 4. (a) Digital image showing [BBR] = 0.2 mM solutions in the presence of various volume fractions of ethanol, and (b) corresponding UV-Visible spectrographs. (c-d) TEM micrographs showing fibers of self-assembled BBR molecules in (c) pure water, and (d) in the presence of 20 vol% ethanol/water. (e) Cryo-TEM micrograph showing BBR fibers formed after incubating the dye solution for 24 h in the crystallization solution containing 1 vol% ethanol. (f and g) Calcite precipitated in the presence of [BBR] = 0.2 mM containing self-assembled dye fibers and (f) 1 vol% and (g) 10 vol% ethanol. The initial pH of the solutions is ≈ 6 and ≈ 9 after mineralization.

Incorporation of alternative soluble additives in binary solvent mixtures

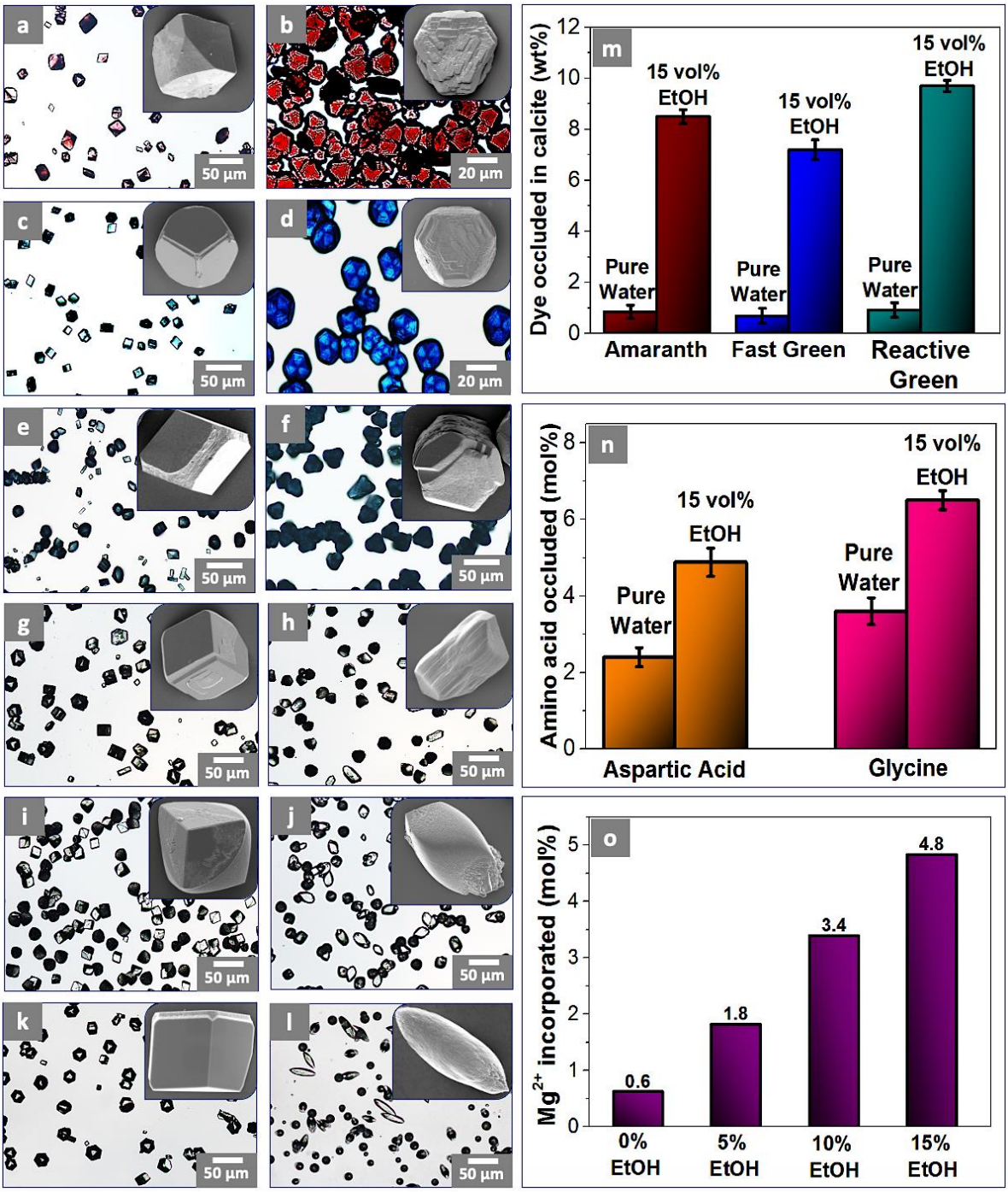

Figure 5. Calcite crystals precipitated in the presence of $[Ca^{2+}]$ = 10 mM and 0.5 mM of (a-b) Amaranth, (c-d) Fast Green and (e-f) Reactive Green dyes in (a, c and e) pure water and (b, d and f) in the presence of 15 vol% ethanol. Calcite precipitated in the presence of $[Ca^{2+}]$ = 10 mM and (g-h) [aspartic acid] = 25 mM, (i-j) [glycine] = 50 mM and (k-l) $[Mg^{2+}]$ = 5 mM in (g, i and k) pure water and (h, j and l) 15 vol% ethanol. Levels of incorporation of the (m) dyes, (n) amino acids and (o) magnesium ions in calcite in pure water and in binary solvent mixtures.

The ability to drive additive incorporation by tuning the composition of the solvent was then extended to alternative additives, where a number of examples are shown in Figure 5 for solutions containing 15 vol% ethanol. Amaranth (a red dye) and Fast Green (a blue dye) both occluded at levels that are 10 times higher than in water alone, and the crystals exhibit pseudo-(001) faces, that are characteristic of preferential interaction with the obtuse steps (Figure 5a-d and Figure 5m). The Fast Green molecules also exhibit an intra-sectorial zoning effect[36, 45, 46] (Figure 5d), and SEM images show that there is no relationship between the zoning pattern and the morphology of the crystals (inset in Figure 5d). Reactive Green (a blue/green dye) incorporated at levels 11 times higher than in pure aqueous system and yielded platonic calcite crystals (Figure 5e-f and Figure 5m).

In addition, we investigated the occlusion of much smaller additives, for which ethanol also promoted the binding of both aspartic acid and glycine to calcite, as evidenced by stronger morphological effects (Figure 5g-j). Thermogravimetric analyses (TGA) revealed a 2-fold increase in incorporation of both amino acids at 15 vol% ethanol (Figure 5n and Figure S5). A comparable effect was observed with magnesium ions, where ethanol enhanced their binding to the calcite surface, causing a characteristic elongation along the *c*-axis (Figure 5k-l and Figure S6).[47-49] Inductively Coupled Plasma – Optical Emission Spectroscopy (ICP – OES) analyses of the composites showed enhanced magnesium inclusion, with amounts of up to ≈ 5 mol% being occluded at 15 vol% ethanol as compared with the modest 0.6 mol% achieved in pure water under the same conditions (Figure 5o).

Comparison with additives performances in pure aqueous solution

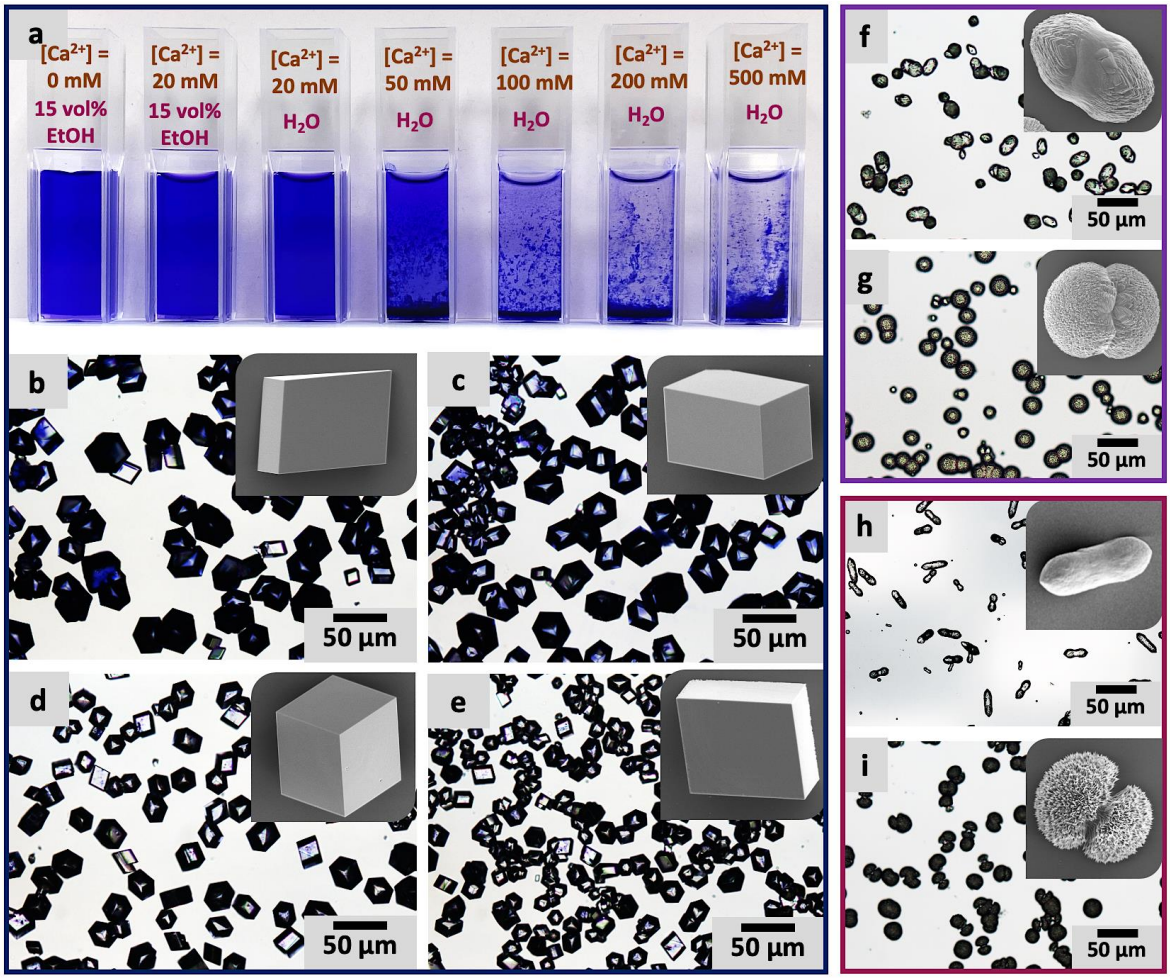

Figure 6. (a) Digital image showing [BBR] = 0.2 mM solutions in the presence of [Ca^{2+}] = 0 mM and 15 vol% ethanol, [Ca^{2+}] = 20 mM and 15 vol% ethanol and [Ca^{2+}] = 20 mM, 50 mM, 100 mM, 200 mM and 500 mM in pure water. Calcite crystals precipitated in the presence of [BBR] = 0.2 mM and (b) [Ca^{2+}] = 50 mM, (c) [Ca^{2+}] = 100 mM, (d) [Ca^{2+}] = 200 mM and (e) [Ca^{2+}] = 500 mM. Insets are SEM images of the precipitated crystals. An increase of the supersaturation failed to promote morphology changes and dye incorporation, where only pale blue calcite rhombs precipitated. Calcite polycrystals precipitated in solutions containing (f) [Ca^{2+}] = 10 mM and [aspartic acid] = 75 mM, and (g) [Ca^{2+}] = 20 mM and [aspartic acid] = 40 mM. (h) Elongated calcite polycrystals precipitated in the presence of [Ca^{2+}] = 10 mM and [Mg^{2+}] = 20 mM, and (i) metastable aragonite polycrystals precipitated in solution containing [Ca^{2+}] = 10 mM and [Mg^{2+}] = 50 mM.

Experiments were also conducted to determine whether the same crystal morphologies and occlusion levels can be achieved in pure aqueous solutions at higher additive concentrations

and solution supersaturations. Considering first BBR, an increase in [Ca^{2+}] from 10 mM to 20 mM and [BBR] from 0.2 mM to 0.5 mM only yielded pale blue calcite crystals containing ≈ 1.3 wt% of dye (Figure 2l), as compared with the 10.5 wt% achieved under the same conditions in solvent mixtures. Further increase in the supersaturation to [Ca^{2+}] = 50 mM (Figure 6b) at [BBR] = 0.2 mM and even [Ca^{2+}] = 100 – 500 mM at [BBR] = 0.5 mM (Figure 6c-e and Figure S7a-d) in pure aqueous solutions also failed to improve the additive performance. Instead, reduced BBR incorporation and morphological effects were observed, as shown by the formation of transparent calcite rhombs. This can be attributed to the dye molecules aggregating in the mineralization solutions containing high [Ca^{2+}] (Figure 6a and Figure S7e).

High additive concentrations of [aspartic acid] = 75 mM in solutions containing [Ca^{2+}] = 10 – 20 mM yielded calcite polycrystals, where the amino acid molecules are accumulated at grain boundaries (Figure 6f and 6g and Figure S8a).[17] In turn, solutions containing [Ca^{2+}] = 10 mM and [Mg^{2+}] = 20 mM generated dumbbell-shaped magnesium calcite polycrystals, while polycrystalline aragonite formed at [Mg^{2+}] = 50 mM (Figure 6h-I and Figure S8b).[50] Higher supersaturations again only support the formation of mixtures of polycrystalline calcite and aragonite particles (Figure S6f). These data conclusively demonstrate that adding a small amount of organic solvent to the crystallization solution significantly enhances the potency of soluble additives, giving access to hybrid single crystals that could not be generated in pure aqueous solutions.

Microstructure of the hybrid single crystals

The impact of incorporated BBR, Fast Green and magnesium ions on the structure of the calcite crystals precipitated from aqueous solution and in the presence of ethanol and dioxane was investigated using synchrotron High-Resolution Powder X-ray Diffraction (HR-PXRD)

(Figure 7). Lattice distortions, microstrain fluctuations, coherence lengths and full width at half-maximum (FWHM) were measured for the (104) reflection of calcite, where these provide information about the additive/mineral interactions. No changes in the peak shape, width or position were observed on adding 15 vol% ethanol or dioxane to the growth solutions (Figure 7a and Figure S9), where large coherence lengths of 650 nm and small microstrains of 0.0035 % were recorded for all samples (Figure S10). It is thus clear from these data that the co-solvents have no effect on the microstructure of calcite.

BBR had little effect on the calcite structure when the crystals were precipitated from aqueous solution, as reflects the low occlusion levels (Figure 7b and Figure 7e-f). Calcite precipitated in the presence of ethanol under conditions Ca = 20 mM, BBR = 0.2 mM and 10 vol% EtOH contained 6.5 wt% BBR. These hybrid crystals showed a four-fold increase in the FWHM (Figure S7d), a reduction of the coherence length to 207 nm, an increase of the microstrain to 0.075%, and lattice expansions of $\Delta a/a \approx 0.027\%$ and $\Delta c/c \approx 0.036\%$. Similar microstructural patterns are also observed for the (006) and (110) reflections of calcite (Figure S11). The larger distortions recorded along the *c*-axis than the *a*-axis are consistent with the anisotropic elasticity of calcite.[17] Even greater effects were observed for calcite crystals precipitated under the same conditions but using dioxane as a co-solvent, rather than ethanol. The product composite crystals contained 10 wt% BBR and small coherence lengths of 120 nm and large microstrains of 0.103% were observed, consistent with the higher BBR content.

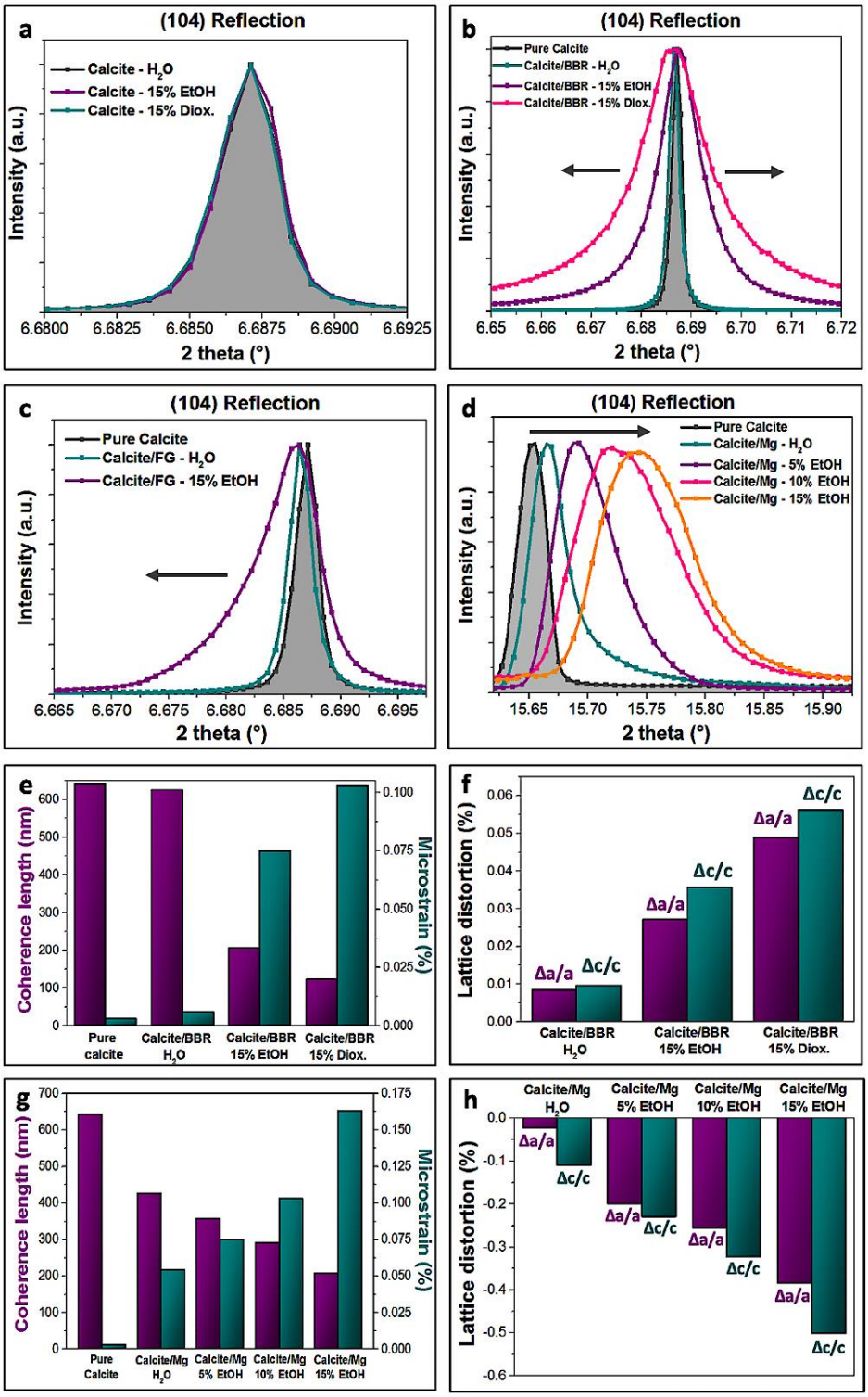

Figure 7. HR-PXRD patterns recorded with (a-c) $\lambda = 0.35449587$ and (d) $\lambda = 0.826764$. (e and g) Coherence lengths and microstrain fluctuations measured for the (104) reflection of pure calcite, and calcite precipitated in the presence of dye molecules and Mg^{2+} ions in aqueous systems and in the presence of organic co-solvents. Lattice distortions along the *a*-axis and *c*-axis of calcite incorporating (f) BBR and (h) Mg in pure aqueous systems and binary solvent mixtures.

Fast Green also had a significant effect on the calcite structure, only when incorporated at the higher levels achievable using co-solvents. Calcite containing 7 wt% Fast Green exhibited a slight shift and asymmetric {104} peaks that extend toward smaller angles, which is indicative of an expansive strain gradient. Interestingly, asymmetric peaks indicative of a compressive strain gradient were previously observed for calcite containing block copolymer micelles.[15] Mg^{2+} ions, in turn, form a solid solution with calcite and shift the diffraction peaks toward higher angles.[51-54] Peak shifts and broadenings are greater at higher levels of magnesium incorporation (Figure 7d) and were thus recorded for calcite precipitated in the presence of ethanol (Figure S10e). Coherence lengths of 200 nm and microstrains of 0.163% were determined for crystals containing ≈ 5 mol% Mg (Figure 7g).

Extension to alternative host crystals

Finally, the versatility of our approach was demonstrated by extending it to the incorporation of Reactive Green in alternative host crystals. In common with the $CaCO_3$ system, little incorporation was achieved in manganese carbonate (rhodochrosite) and strontium sulfate (celestine) precipitated from pure aqueous solutions (Figure 8, Figure S12 and Figure S13). The introduction of ethanol into the mineralization solutions promoted dye incorporation, as evidenced by the formation of darker blue/green crystals, and TGA analyses which confirmed a 2.5-fold increase in occlusion (Figure S14 and Figure S15). The morphologies of the crystals were also altered in the binary solvent mixtures, demonstrating an enhanced binding affinity of the dye molecules to the crystals in the presence of ethanol. We stress that our approach does not allow only an optimization of the experimental conditions, but actually enables access to control over the morphology, structure and composition of various hybrid materials that we are unable to achieve in its absence.

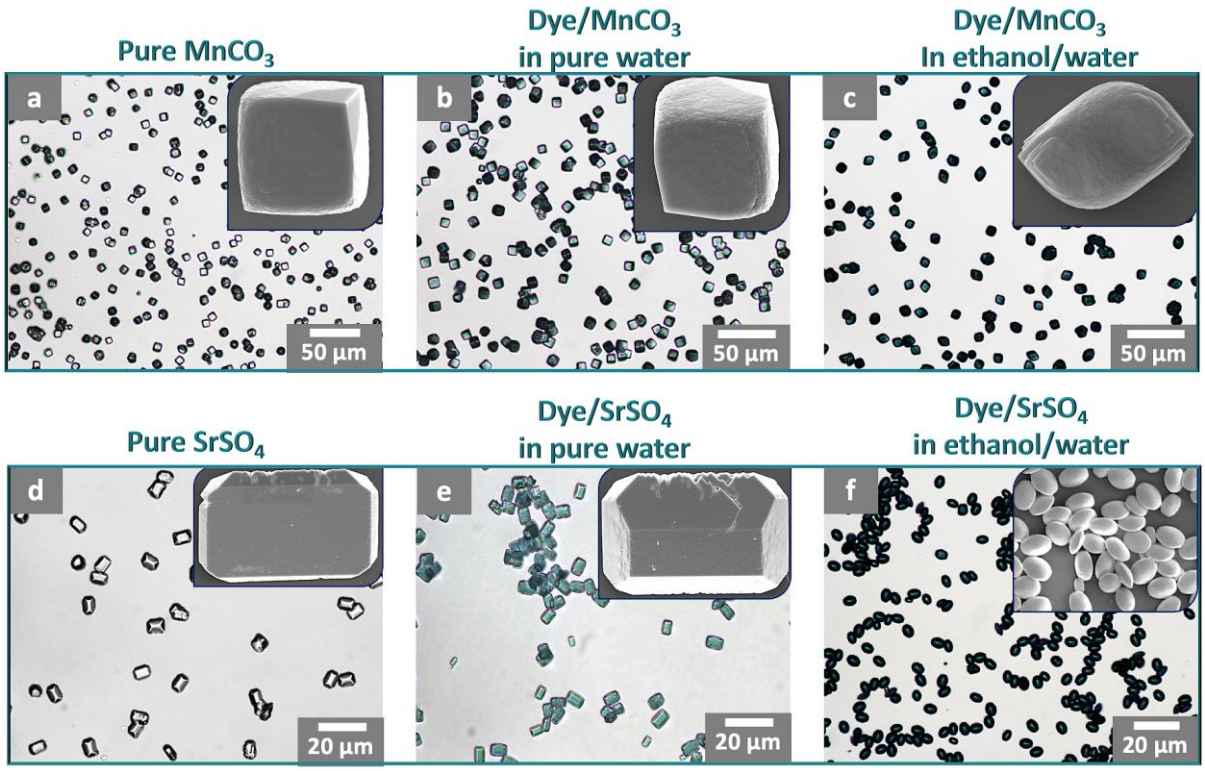

Figure 8. (a) $MnCO_3$ and (d) $SrSO_4$ crystals precipitated from aqueous solution. (b and c) $MnCO_3$ crystals precipitated in the presence of Reactive Green dye in (b) water and (c) 10 vol% ethanol. (e and f) $SrSO_4$ crystals precipitated in the presence of Reactive Green in (e) pure water and (f) 10 vol% ethanol/water. Insets are the SEM images of the crystals.

DISCUSSION

A number of experimental and modelling studies have investigated the formation of calcium carbonate from alcohol/water mixtures. ACC is the first phase formed in most experimental systems and is significantly stabilized in the presence of alcohol. This is attributed to strong binding of organic molecules to the surfaces of the ACC particles due to hydrogen bonds between the OH group on the alcohol and the carbonate oxygen atom,[34, 35] and electrostatic interactions between the hydroxyl oxygen atom and the calcium ion.[55] This delays the precipitation of crystalline phases *via* a dissolution-reprecipitation mechanism. Solvent mixtures can also direct the crystallization pathway of calcium carbonate, resulting in a polymorph switch from the thermodynamically stable calcite toward the kinetic polymorphs

vaterite and aragonite.[24, 26, 27] Crystallization in organic solvents containing traces of water favors metastable phases due to the reduced solubility of $CaCO_3$.[56 57] However, the polymorph distribution is highly dependent on variables including the stirring rate, temperature and the alcohol/water ratio, where significant quantities of vaterite or aragonite are usually only achieved using high ratios of alcohol (> 50 vol%).[24]

Numerous studies have shown that co-solvents such as alcohols can strongly influence the structural water layer present on the calcite surface.[55, 58, 59] Alcohols bind more strongly than water molecules, and thus displace the water to create a highly ordered alcohol layer with the aliphatic tails oriented away from the mineral surface.[55, 58] This alcohol layer changes the charge and wettability of the calcite surface, significantly hindering mass transport to the mineral surface, and retarding growth and dissolution.[58, 60] However, simulations have shown that the ordering of the alcohol molecules is disrupted near the step edges,[60, 61] and that disrupted water dominates at this location.[61] This creates an essential bridge between the bulk solution and step edges, which enables solutes and additives to access these active sites and allows the crystal to grow and incorporate guest species.[35, 60]

Our results clearly demonstrate that small quantities (under 15 vol%) of a range of co-solvents can strongly affect the interactions of soluble additives with calcite, as evidenced by the enhanced morphological changes and occlusion levels. These effects increase as the dielectric constant and polarity of the co-solvent decrease,[40, 41] and are likely to derive from a range of factors. The organic solvent reduces the solubility of additives in the mineralization solution. For example, addition of 5 – 15 vol% of ethanol decreases the solubility of glycine by 10 – 30%.[62, 63] Although too small to induce precipitation of glycine, this could be sufficient to increase the flux of the amino acid to the crystal/solution interface. The solution supersaturation

is also higher in the solvent mixtures, which increases the step density and thus the growth rate of the smooth {104} faces. This enhances the expression of pseudo-faces where additives occlude at higher rates. Similarly, an increased kink density is expected, which improves the probability of an adsorbate becoming kinetically trapped and occluded.[14, 37, 45, 48] This increase in supersaturation is greater in organic solvents with longer aliphatic chains, which could explain the enhanced levels of incorporation in solvent mixtures with lower polarities.[57] Increasing the amount of organic co-solvent in the mineralization solution also facilitates dehydration of the $CaCO_3$ solutes and additives, which must occur prior to their incorporation within the calcite lattice.[5, 50, 64 65-67]

Finally, additive/crystal interactions are governed by the adsorption thermodynamics of the additives, which must compete with the solvent for access to the crystal growth sites.[68, 69] As the organic co-solvents affect both the solubility of the additives and the solvent structure at the crystal surface, these effects may both increase the flux of additives to the mineral surface and reduce their detachment rates, leading to a higher additive coverage. An increased additive coverage means that more additives are available for occlusion, and that the growth rates of the crystal surfaces are reduced, leading to an enhanced morphological effect. The structural water layer adsorbed on the crystal surface also hinders the access of additive to the binding sites of the mineral by shielding the additive/crystal electrostatic forces. Disruption of this water layer by the organic solvent facilitates the binding of additives and their incorporation in the crystals.

CONCLUSIONS

Many applications of inorganic crystals require the production of particles with specific morphologies, sizes, structures, and polymorphs, a need that is often met using soluble additives. We have demonstrated that the ability of additives to direct crystallization in aqueous

solution can be significantly enhanced through the addition of small quantities of miscible co-solvents. While it is recognized that co-solvents can exert some influence over the polymorph of compounds such as calcium carbonate, our results show that solvent mixtures significantly enhance the interaction between additives and crystals, and thus offer a powerful means of precisely tuning both the occlusion of additives within host crystals, and modifying crystal morphologies. These results were valid for a wide variety of additives, co-solvents and host crystals, indicating a general underlying mechanism. As future work, molecular simulations could be used to gain further insight into additive/crystal interactions, but this is non-trivial and beyond the scope of the current project, as force fields do not currently exist for the relevant solvation free energies. Our work also suggests that soluble additives may have enhanced effects on crystallization in environments where the water activity is low, such as in nanoporous media or biological systems. This versatile approach is expected to find applications in a plethora of fields including crystal synthesis, oil recovery, drug storage, and contamination remediation.

EXPERIMENTAL SECTION

$CaCO_3$ mineralization in the presence of soluble additives in pure water and binary solvent mixtures: Calcium carbonate ($CaCO_3$) was precipitated using the ammonium carbonate diffusion method,[31] in the presence of the soluble additives (*i.e.,* ions, amino acids or dye molecules), both in pure aqueous solution and in the presence of varying amounts (0 – 75 vol%) of organic co-solvents (*i.e.,* methanol, ethanol, 1-proparnol, 2-propanol or dioxane. Piranha cleaned glass substrates were deposited at the bottom of a well-plate containing a total volume of 1 mL of solution. Desired amounts of additives were introduced in mineralization medium containing [Ca^{2+}] = 10 mM – 500 mM, in pure aqueous solutions or in the presence of 5 – 75 vol% of co-solvents. Calcification in the presence of the additives was carried out by placing

the reaction mixtures inside a sealed desiccator, containing 2 g of $(NH_4)_2CO_3$, placed in a Petri-dish and covered with Parafilm punctured several times with a needle. Mineralization was allowed to proceed overnight (> 12 h). After reaction completion, the substrates supporting the crystals were washed several times with DI water and then ethanol, followed by gentle drying using N_2(g) stream, prior to characterization.

Precipitation of $MnCO_3$ and $SrSO_4$ in the presence of Reactive Green, in pure water and binary solvent mixtures: Rhodochrosite ($MnCO_3$) and celestine ($SrSO_4$) were precipitated by mixing equal volumes of $[Mn^{2+}]$ = 2 mM and $[NaHCO_3]$ = 200 mM, and $[Sr^{2+}]$ = 4 mM and $[Na_2SO_4]$ = 20 mM, respectively. Piranha cleaned glass substrates were deposited at the bottom of a well-plate containing a total volume of 1 mL of solution. [Reactive Green] = 0.05 mM was introduced in the $MnCO_3$ and $SrSO_4$ mineralization solutions in both pure aqueous solutions and in the presence of 10 vol% of ethanol. Mineralization was allowed to proceed overnight (> 12 h). After reaction completion, the substrates supporting the crystals were carefully washed several times with DI water and then ethanol, followed by drying using N_2(g) stream, prior to characterization.

Characterization: The samples were characterized using a combination of analytical techniques including Raman, Fourier-Transform Infrared (FTIR) spectroscopy, Inductively Coupled Plasma - Optical Emission Spectroscopy (ICP-OES), Atomic Absorption and UV-Visible spectroscopy, synchrotron High-Resolution Powder XRD (HR-PXRD), thermogravimetric analysis (TGA), and optical and electron microscopy (cryo-TEM, dry TEM and SEM). Further details are provided in the Supporting Information.

ASSOCIATED CONTENT

Supporting Information

Experimental details including the synthesis of the hybrid crystals, analytic methodologies, FTIR, UV-Visible, HR-PXRD, TGA analyses, and additional optical and SEM micrographs.

AUTHOR INFORMATION

Corresponding Authors

Ouassef Nahi, School of Chemistry, University of Leeds, Woodhouse Lane, Leeds, LS2 9JT, UK.

Email: pmona@leeds.ac.uk

Fiona Meldrum, School of Chemistry, University of Leeds, Woodhouse Lane, Leeds, LS2 9JT, UK.

Email: f.meldrum@leeds.ac.uk

Authors

Alexander N. Kulak, School of Chemistry, University of Leeds, Woodhouse Lane, Leeds, LS2 9JT, UK.

Alexander Broad, London Centre for Nanotechnology, Department of Physics and Astronomy, University College London, Gower Street, London WC1E 6BT, UK.

Yifei Xu, School of Chemistry, University of Leeds, Woodhouse Lane, Leeds, LS2 9JT, UK.

Cedrick O'Shaughnessy, School of Chemistry, University of Leeds, Woodhouse Lane, Leeds, LS2 9JT, UK.

Olivier J. Cayre, School of Chemical and Process Engineering, University of Leeds, Woodhouse Lane, Leeds, LS2 9JT, UK.

Sarah J. Day, Diamond Light Source, Harwell Science and Innovation Campus, Harwell, Didcot, Oxfordshire, OX11 0DE, UK

Robert Darkins, London Centre for Nanotechnology, Department of Physics and Astronomy, University College London, Gower Street, London WC1E 6BT, UK.

Author Contributions

The manuscript was written through contributions of all authors. All authors have given approval to the final version of the manuscript.

Funding sources

This research was funded, in whole or in part, by [EPSRC, EP/L015285/1, EP/R018820/1, EP/N002423/1] and [Leverhulme Trust, RPG-2017-178]. For the purpose of open access, the author has applied a CC-BY public copyright license to any Author Accepted Manuscript (AAM) version arising from this submission.

Notes

The authors declare no competing financial interest.

ACKNOWLEDGMENTS

We thank the European Synchrotron Radiation Facility (ESRF – beamline ID22; proposal CH5905) and Diamond Light Source (beamline I11; proposal CY27557) for beamtimes and the assistance provided by the personnel (Dr. Ola G. Grendal and Dr. Sarah J. Day). We are also thankful to the Leeds Electron Microscopy and Spectroscopy Centre (LEMAS) and Astbury Biostructure Laboratory (ABL) for access and support from the electron microscopy facilities.

REFERENCES

(1) Sun, J.; Bhushan, B., Hierarchical structure and mechanical properties of nacre: a review. *RSC Adv.* **2012,** 2, (20), 7617-7632.

(2) Aizenberg, J.; Tkachenko, A.; Weiner, S.; Addadi, L.; Hendler, G., Calcitic microlenses as part of the photoreceptor system in brittlestars. *Nature* **2001,** 412, (6849), 819-22.

(3) Aizenberg, J.; Weaver, J. C.; Thanawala, M. S.; Sundar, V. C.; Morse, D. E.; Fratzl, P., Skeleton of Euplectella sp.: Structural Hierarchy from the Nanoscale to the Macroscale. *Science* **2005,** 309, (5732), 275-278.

(4) Loste, E.; Wilson, R. M.; Seshadri, R.; Meldrum, F. C., The role of magnesium in stabilising amorphous calcium carbonate and controlling calcite morphologies. *J. Cryst. Growth* **2003,** 254, (1), 206-218.

(5) Davis, K. J.; Dove, P. M.; De Yoreo, J. J., The role of Mg2+ as an impurity in calcite growth. *Science* **2000,** 290, (5494), 1134-7.

(6) Hodkin, D. J.; Stewart, D. I.; Graham, J. T.; Cibin, G.; Burke, I. T., Enhanced Crystallographic Incorporation of Strontium(II) Ions into Calcite via Preferential Adsorption at Obtuse Growth Steps. *Cryst. Growth Des.* **2018,** 18, (5), 2836-2843.

(7) Wasylenki, L. E.; Dove, P. M.; Wilson, D. S.; De Yoreo, J. J., Nanoscale effects of strontium on calcite growth: An in situ AFM study in the absence of vital effects. *Geochim. Cosmochim. Acta* **2005,** 69, (12), 3017-3027.

(8) Aquilano, D.; Bruno, M.; Pastero, L., Impurity Effects on Habit Change and Polymorphic Transitions in the System: Aragonite–Calcite–Vaterite. *Cryst. Growth Des.* **2020,** 20, (4), 2497-2507.

(9) Cölfen, H.; Antonietti, M., Crystal Design of Calcium Carbonate Microparticles Using Double-Hydrophilic Block Copolymers. *Langmuir* **1998,** 14, (3), 582-589.

(10) Zhao, K.; Wang, M.; Wang, X.; Wu, C.; Xu, H.; Lu, J. R., Crystal Growth of Calcite Mediated by Ovalbumin and Lysozyme: Atomic Force Microscopy Study. *Cryst. Growth Des.* **2013,** 13, (4), 1583-1589.

(11) Butler, M. F.; Glaser, N.; Weaver, A. C.; Kirkland, M.; Heppenstall-Butler, M., Calcium Carbonate Crystallization in the Presence of Biopolymers. *Cryst. Growth Des.* **2006,** 6, (3), 781-794.

(12) Yang, M.; Stipp, S. L. S.; Harding, J., Biological Control on Calcite Crystallization by Polysaccharides. *Cryst. Growth Des.* **2008,** 8, (11), 4066-4074.

(13) Verch, A.; Gebauer, D.; Antonietti, M.; Cölfen, H., How to control the scaling of CaCO3: a "fingerprinting technique" to classify additives. *Phys. Chem. Chem. Phys.* **2011,** 13, (37), 16811-16820.

(14) Kim, Y.-Y.; Fielding, L. A.; Kulak, A. N.; Nahi, O.; Mercer, W.; Jones, E. R.; Armes, S. P.; Meldrum, F. C., Influence of the Structure of Block Copolymer Nanoparticles on the Growth of Calcium Carbonate. *Chem. Mater.* **2018,** 30, (20), 7091-7099.

(15) Kim, Y.-Y.; Ganesan, K.; Yang, P.; Kulak, A. N.; Borukhin, S.; Pechook, S.; Ribeiro, L.; Kröger, R.; Eichhorn, S. J.; Armes, S. P.; Pokroy, B.; Meldrum, F. C., An artificial biomineral formed by incorporation of copolymer micelles in calcite crystals. *Nat. Mater.* **2011,** 10, (11), 890-896.

(16) Kim, Y.-Y.; Darkins, R.; Broad, A.; Kulak, A. N.; Holden, M. A.; Nahi, O.; Armes, S. P.; Tang, C. C.; Thompson, R. F.; Marin, F.; Duffy, D. M.; Meldrum, F. C., Hydroxyl-rich macromolecules enable the bio-inspired synthesis of single crystal nanocomposites. *Nat. Commun.* **2019,** 10, (1), 5682.

(17) Kim, Y.-Y.; Carloni, J. D.; Demarchi, B.; Sparks, D.; Reid, D. G.; Kunitake, Miki E.; Tang, C. C.; Duer, M. J.; Freeman, C. L.; Pokroy, B.; Penkman, K.; Harding, J. H.; Estroff, L. A.; Baker,

S. P.; Meldrum, F. C., Tuning hardness in calcite by incorporation of amino acids. *Nat. Mater.* **2016,** 15, (8), 903-910.

(18) Kulak, A. N.; Semsarilar, M.; Kim, Y.-Y.; Ihli, J.; Fielding, L. A.; Cespedes, O.; Armes, S. P.; Meldrum, F. C., One-pot synthesis of an inorganic heterostructure: uniform occlusion of magnetite nanoparticles within calcite single crystals. *Chem. Sci.* **2014,** 5, (2), 738-743.

(19) Liu, Y.; Zang, H.; Wang, L.; Fu, W.; Yuan, W.; Wu, J.; Jin, X.; Han, J.; Wu, C.; Wang, Y.; Xin, H. L.; Chen, H.; Li, H., Nanoparticles Incorporated inside Single-Crystals: Enhanced Fluorescent Properties. *Chem. Mater.* **2016,** 28, (20), 7537-7543.

(20) Green, D. C.; Holden, M. A.; Levenstein, M. A.; Zhang, S.; Johnson, B. R. G.; Gala de Pablo, J.; Ward, A.; Botchway, S. W.; Meldrum, F. C., Controlling the fluorescence and room-temperature phosphorescence behaviour of carbon nanodots with inorganic crystalline nanocomposites. *Nat. Commun.* **2019,** 10, (1), 206.

(21) Reischl, B.; Raiteri, P.; Gale, J. D.; Rohl, A. L., Atomistic Simulation of Atomic Force Microscopy Imaging of Hydration Layers on Calcite, Dolomite, and Magnesite Surfaces. *J. Phys. Chem. C* **2019,** 123, (24), 14985-14992.

(22) Miyazawa, K.; Tracey, J.; Reischl, B.; Spijker, P.; Foster, A. S.; Rohl, A. L.; Fukuma, T., Tip dependence of three-dimensional scanning force microscopy images of calcite–water interfaces investigated by simulation and experiments. *Nanoscale* **2020,** 12, (24), 12856-12868.

(23) Nakouzi, E.; Stack, A. G.; Kerisit, S.; Legg, B. A.; Mundy, C. J.; Schenter, G. K.; Chun, J.; De Yoreo, J. J., Moving beyond the Solvent-Tip Approximation to Determine Site-Specific Variations of Interfacial Water Structure through 3D Force Microscopy. *J. Phys. Chem. C* **2021,** 125, (2), 1282-1291.

(24) Sand, K. K.; Rodriguez-Blanco, J. D.; Makovicky, E.; Benning, L. G.; Stipp, S. L. S., Crystallization of CaCO3 in Water–Alcohol Mixtures: Spherulitic Growth, Polymorph Stabilization, and Morphology Change. *Cryst. Growth Des.* **2012,** 12, (2), 842-853.

(25) Manoli, F.; Dalas, E., Spontaneous precipitation of calcium carbonate in the presence of ethanol, isopropanol and diethylene glycol. *J. Cryst. Growth* **2000,** 218, (2), 359-364.

(26) Chen, S.-F.; Yu, S.-H.; Jiang, J.; Li, F.; Liu, Y., Polymorph Discrimination of CaCO3 Mineral in an Ethanol/Water Solution: Formation of Complex Vaterite Superstructures and Aragonite Rods. *Chem. Mater.* **2006,** 18, (1), 115-122.

(27) Dickinson, S. R.; McGrath, K. M., Switching between kinetic and thermodynamic control: calcium carbonate growth in the presence of a simple alcohol. *J. Mater. Chem.* **2003,** 13, (4), 928-933.

(28) Seo, K.-S.; Han, C.; Wee, J.-H.; Park, J.-K.; Ahn, J.-W., Synthesis of calcium carbonate in a pure ethanol and aqueous ethanol solution as the solvent. *J. Cryst. Growth* **2005,** 276, (3), 680-687.

(29) Ning, Y.; Han, L.; Derry, M. J.; Meldrum, F. C.; Armes, S. P., Model Anionic Block Copolymer Vesicles Provide Important Design Rules for Efficient Nanoparticle Occlusion within Calcite. *J. Am. Chem. Soc.* **2019,** 141, (6), 2557-2567.

(30) Elhadj, S.; Salter, E. A.; Wierzbicki, A.; De Yoreo, J. J.; Han, N.; Dove, P. M., Peptide Controls on Calcite Mineralization: Polyaspartate Chain Length Affects Growth Kinetics and Acts as a Stereochemical Switch on Morphology. *Cryst. Growth Des.* **2006,** 6, (1), 197-201.

(31) Ihli, J.; Bots, P.; Kulak, A.; Benning, L. G.; Meldrum, F. C., Elucidating Mechanisms of Diffusion-Based Calcium Carbonate Synthesis Leads to Controlled Mesocrystal Formation. *Adv. Funct. Mater.* **2013,** 23, (15), 1965-1973.

(32) Gindele, M. B.; Steingrube, L. V.; Gebauer, D., Generality of liquid precursor phases in gas diffusion-based calcium carbonate synthesis. *CrystEngComm* **2021**, 1-6.

(33) Rao, A.; Huang, Y.-C.; Cölfen, H., Additive Speciation and Phase Behavior Modulating Mineralization. *J. Phys. Chem. C* **2017,** 121, (39), 21641-21649.

(34) Chen, S.-F.; Cölfen, H.; Antonietti, M.; Yu, S.-H., Ethanol assisted synthesis of pure and stable amorphous calcium carbonate nanoparticles. *ChemComm* **2013,** 49, (83), 9564-9566.

(35) Lee, H. S.; Ha, T. H.; Kim, K., Fabrication of unusually stable amorphous calcium carbonate in an ethanol medium. *Mater. Chem. Phys.* **2005,** 93, (2), 376-382.

(36) Marzec, B.; Green, D. C.; Holden, M. A.; Coté, A. S.; Ihli, J.; Khalid, S.; Kulak, A.; Walker, D.; Tang, C.; Duffy, D. M.; Kim, Y.-Y.; Meldrum, F. C., Amino Acid Assisted Incorporation of Dye Molecules within Calcite Crystals. *Angew. Chem. Int. Ed.* **2018,** 57, (28), 8623-8628.

(37) Rae Cho, K.; Kim, Y.-Y.; Yang, P.; Cai, W.; Pan, H.; Kulak, A. N.; Lau, J. L.; Kulshreshtha, P.; Armes, S. P.; Meldrum, F. C.; De Yoreo, J. J., Direct observation of mineral–organic composite formation reveals occlusion mechanism. *Nat. Commun.* **2016,** 7, (1), 10187.

(38) Kulak, A. N.; Iddon, P.; Li, Y.; Armes, S. P.; Cölfen, H.; Paris, O.; Wilson, R. M.; Meldrum, F. C., Continuous Structural Evolution of Calcium Carbonate Particles: A Unifying Model of Copolymer-Mediated Crystallization. *J. Am. Chem. Soc.* **2007,** 129, (12), 3729-3736.

(39) Smeets, P. J. M.; Cho, K. R.; Sommerdijk, N. A. J. M.; De Yoreo, J. J., A Mesocrystal-Like Morphology Formed by Classical Polymer-Mediated Crystal Growth. *Adv. Funct. Mater.* **2017,** 27, (40), 1701658.

(40) Akerlof, G.; Short, O. A., The Dielectric Constant of Dioxane—Water Mixtures between 0 and 80°. *J. Am. Chem. Soc.* **1936,** 58, (7), 1241-1243.

(41) Akerlof, G., Dielectric constants of some organic solvent-water mixtures at various temperatures. *J. Am. Chem. Soc.* **1932,** 54, (11), 4125-4139.

(42) Von Berlepsch, H.; Kirstein, S.; Böttcher, C., Effect of Alcohols on J-Aggregation of a Carbocyanine Dye. *Langmuir* **2002,** 18, (20), 7699-7705.

(43) Mera, S. L.; Davies, J. D., Differential Congo Red staining: The effects of pH, non-aqueous solvents and the substrate. *Histochem J.* **1984,** 16, (2), 195-210.

(44) Bujdák, J., The effects of layered nanoparticles and their properties on the molecular aggregation of organic dyes. *J. Photochem. Photobiol. C* **2018,** 35, 108-133.

(45) Green, D. C.; Ihli, J.; Thornton, P. D.; Holden, M. A.; Marzec, B.; Kim, Y.-Y.; Kulak, A. N.; Levenstein, M. A.; Tang, C.; Lynch, C.; Webb, S. E. D.; Tynan, C. J.; Meldrum, F. C., 3D visualization of additive occlusion and tunable full-spectrum fluorescence in calcite. *Nat. Commun.* **2016,** 7, (1), 13524.

(46) Ihli, J.; Levenstein, M. A.; Kim, Y.-Y.; Wakonig, K.; Ning, Y.; Tatani, A.; Kulak, A. N.; Green, D. C.; Holler, M.; Armes, S. P.; Meldrum, F. C., Ptychographic X-ray tomography reveals additive zoning in nanocomposite single crystals. *Chem. Sci.* **2020,** 11, (2), 355-363.

(47) Davis, K. J.; Dove, P. M.; Wasylenki, L. E.; De Yoreo, J. J., Morphological consequences of differential Mg2+ incorporation at structurally distinct steps on calcite. *Am. Mineral.* **2004,** 89, (5-6), 714-720.

(48) Kim, Y.-Y.; Freeman, C. L.; Gong, X.; Levenstein, M. A.; Wang, Y.; Kulak, A.; Anduix-Canto, C.; Lee, P. A.; Li, S.; Chen, L.; Christenson, H. K.; Meldrum, F. C., The Effect of Additives on the Early Stages of Growth of Calcite Single Crystals. *Angew. Chem. Int. Ed.* **2017,** 56, (39), 11885-11890.

(49) Albeck, S.; Aizenberg, J.; Addadi, L.; Weiner, S., Interactions of various skeletal intracrystalline components with calcite crystals. *J. Am. Chem. Soc.* **1993,** 115, (25), 11691-11697.

(50) Sun, W.; Jayaraman, S.; Chen, W.; Persson, K. A.; Ceder, G., Nucleation of metastable aragonite CaCO3 in seawater. *Proc. Natl. Acad. Sci. U.S.A.* **2015,** 112, (11), 3199-3204.

(51) Seknazi, E.; Pokroy, B., Residual Strain and Stress in Biocrystals. *Adv. Mater.* **2018,** 30, (41), 1707263.

(52) Zolotoyabko, E.; Caspi, E. N.; Fieramosca, J. S.; Von Dreele, R. B.; Marin, F.; Mor, G.; Addadi, L.; Weiner, S.; Politi, Y., Differences between Bond Lengths in Biogenic and Geological Calcite. *Cryst. Growth Des.* **2010,** 10, (3), 1207-1214.

(53) Polishchuk, I.; Bracha, A. A.; Bloch, L.; Levy, D.; Kozachkevich, S.; Etinger-Geller, Y.; Kauffmann, Y.; Burghammer, M.; Giacobbe, C.; Villanova, J.; Hendler, G.; Sun, C.-Y.; Giuffre, A. J.; Marcus, M. A.; Kundanati, L.; Zaslansky, P.; Pugno, N. M.; Gilbert, P. U. P. A.; Katsman, A.; Pokroy, B., Coherently aligned nanoparticles within a biogenic single crystal: A biological prestressing strategy. *Science* **2017,** 358, (6368), 1294.

(54) Pokroy, B.; Fitch, A. N.; Marin, F.; Kapon, M.; Adir, N.; Zolotoyabko, E., Anisotropic lattice distortions in biogenic calcite induced by intra-crystalline organic molecules. *J. Struct. Biol.* **2006,** 155, (1), 96-103.

(55) Bovet, N.; Yang, M.; Javadi, M. S.; Stipp, S. L. S., Interaction of alcohols with the calcite surface. *Phys. Chem. Chem. Phys.* **2015,** 17, (5), 3490-3496.

(56) Ryu, M.; Ahn, J.; You, K.; Goto, S.; Kim, H., Synthesis of calcium carbonate in ethanol-ethylene glycol solvent. *J. Ceram. Soc. Japan* **2009,** 117, (1361), 106-110.

(57) Magnabosco, G.; Polishchuk, I.; Pokroy, B.; Rosenberg, R.; Cölfen, H.; Falini, G., Synthesis of calcium carbonate in trace water environments. *ChemComm* **2017,** 53, (35), 4811-4814.

(58) Hakim, S. S.; Olsson, M. H. M.; Sørensen, H. O.; Bovet, N.; Bohr, J.; Feidenhans'l, R.; Stipp, S. L. S., Interactions of the Calcite {10.4} Surface with Organic Compounds: Structure and Behaviour at Mineral – Organic Interfaces. *Sci. Rep.* **2017,** 7, (1), 7592.

(59) Budi, A.; Stipp, S. L. S.; Andersson, M. P., The effect of solvation and temperature on the adsorption of small organic molecules on calcite. *Phys. Chem. Chem. Phys.* **2018,** 20, (10), 7140-7147.

(60) Keller, K. S.; Olsson, M. H. M.; Yang, M.; Stipp, S. L. S., Adsorption of Ethanol and Water on Calcite: Dependence on Surface Geometry and Effect on Surface Behavior. *Langmuir* **2015,** 31, (13), 3847-3853.

(61) Pasarín, I. S.; Yang, M.; Bovet, N.; Glyvradal, M.; Nielsen, M. M.; Bohr, J.; Feidenhans'l, R.; Stipp, S. L. S., Molecular Ordering of Ethanol at the Calcite Surface. *Langmuir* **2012,** 28, (5), 2545-2550.

(62) Bowden, N. A.; Sanders, J. P. M.; Bruins, M. E., Solubility of the Proteinogenic α-Amino Acids in Water, Ethanol, and Ethanol–Water Mixtures. *J. Chem. Eng. Data* **2018,** 63, (3), 488-497.

(63) Ji, P.; Zou, J.; Feng, W., Effect of alcohol on the solubility of amino acid in water. *J. Mol. Catal. B Enzym.* **2009,** 56, (2), 185-188.

(64) Folk, R. L., The natural history of crystalline calcium carbonate; effect of magnesium content and salinity. *J. Sediment. Res.* **1974,** 44, (1), 40-53.

(65) Song, X.; Dai, C.; Chen, G.; Dong, C.; Yu, J., Effect of alcohol on the crystallization process of MgCO3·3H2O: an experimental and molecular dynamics simulation study. *Energy Sources A: Recovery Util. Environ. Eff.* **2020,** 42, (9), 1118-1131.

(66) Oomori, T.; Kitano, Y., Synthesis of protodolomite from sea water containing dioxane. *Geochem. J.* **1987,** 21, (2), 59-65.

(67) Falini, G.; Gazzano, M.; Ripamonti, A., Magnesium calcite crystallizatin from water–alcohol mixtures. *ChemComm* **1996**, (9), 1037-1038.

(68) De Yoreo, J. J.; Vekilov, P. G., Principles of Crystal Nucleation and Growth. *Rev. Mineral. Geochem.* **2003,** 54, (1), 57-93.

(69) Sangwal, K., Additives and Crystallization Processes: From Fundamentals to Applications. In John Wiley & Sons: Chichester, **2007**.

For Table of Contents Use Only

Solvent-Mediated Enhancement of Additive-Controlled Crystallization

Ouassef Nahi,* Alexander N. Kulak, Alexander Broad, Yifei Xu, Cedrick O'Shaughnessy, Olivier J. Cayre, Sarah J. Day, Robert Darkins, and Fiona C. Meldrum*

Addition of small amounts of organic co-solvents to an aqueous crystallization solution significantly enhances the effects of soluble additives, generating striking changes in crystal morphologies and considerable increases in additive incorporation. This is realized by tuning the physico-chemical properties of the solution, enabling the facile access to composite materials with tailored shapes, structures, and compositions that are unachievable from pure aqueous systems.